ECMWF Feature article

from Newsletter Number 105 – Autumn 2005

METEOROLOGY

The local and global impact of the recent change in model aerosol climatology

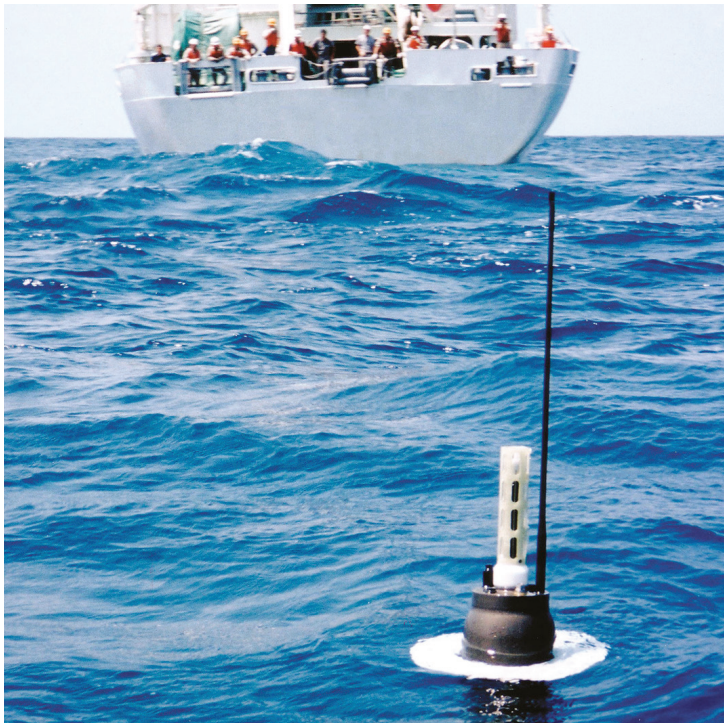

www.ecmwf.int/en/about/news-centre/media-resources

doi:10.21957/345mr1psx6

This article appeared in the Meteorology section of ECMWF Newsletter No. 105 – Autumn 2005, pp. 17–23.

The local and global impact of the recent change in model aerosol climatology

Mark Rodwell

The impact of aerosol on local air quality and climate change is becoming an important topic of research. This is particularly the case for Asia where the so-called "Asian Brown Cloud" causes major health concerns and may have serious agricultural and economic consequences if aerosol can influence the climatological monsoon circulation. With these concerns in mind the ECMWF-coordinated "GEMS" project aims to improve our knowledge of atmospheric aerosol distribution (for further information see the article by Tony Hollingsworth in *ECMWF Newsletter No. 103*).

Here the impacts of a recent change in model aerosol climatology are investigated. It is found that the aerosol change (which is predominantly over North Africa) does influence the climatological North African monsoon circulation. In addition, it also has far wider impacts: affecting the winter extratropical circulation of each hemisphere and leading to improvements in medium-range forecast skill. These results suggest that the GEMS project could lead to further numerical weather prediction improvements and necessary advances in our understanding of climate change.

The old and new model aerosol climatologies

Until recently the aerosol climatology used in the ECMWF operational forecasting model (up to and including cycle Cy26r1) was based on that of *Tanre et al.* (1984). This climatology is specified as annual mean geographical distributions of various aerosol types: "maritime", "continental", "urban", "desert" and uniformly distributed stratospheric background aerosols, all with fixed vertical distributions. Figure 1(a) shows the geographical distribution of the total aerosol optical depth at 550 nm (an optical depth of d for a particular wavelength attenuates radiation at that wavelength by a factor e^{-d} as it passes through the atmosphere). The maximum optical depth (0.74) is seen to occur over the Sahara and this is dominated by desert (sand dust) aerosol.

Over the last two decades, chemical and transport models, which are able to represent the life cycles of different aerosol types, have been used to create an inventory of their spatial and temporal distributions. Out of these studies, a new climatology for the annual cycle in each aerosol type has been compiled by *Tegen et al.* (1997). This climatology was implemented in the ECMWF forecast system at cycle Cy26r3 in October 2003. The new aerosol climatology for July (Figure 1(c)) is still dominated by sand dust but the region of maximum total optical depth (maximising at a value of 1.05) is now located over the Horn of Africa and out into the Arabian Sea associated with the transport of dust by the monsoonal Somali Jet. The aerosol optical depth over the Sahara is greatly reduced. The January aerosol of the new climatology (Figure 1(b)) also shows major differences with the old annual mean climatology (Figure 1(a)).

Tanre et al. (1984) investigated the impact of introducing aerosol into the ECMWF model; here the local and global impacts of the recent change in the aerosol climatology are discussed.

Impact on seasonal systematic errors (June–August)

Seasonal simulations have been made with the old and new aerosol, based on model version Cy26r3 run at T95 resolution and started from 1 April for the years 1962–2001 from ERA-40 analyses. Figure 2(a) shows mean June–August precipitation, low-level (925 hPa) winds and 500 hPa geopotential heights from the observations. The summer monsoons of southern Asia, North Africa and Mexico, together with their associated low-level inflows are clearly evident. In the extratropics, a weak (strong) westerly jet is evident from the tightness of the geopotential height contours in the summer (winter) hemisphere. The statistically significant systematic errors associated with the old aerosol (Figure 2(b)) include too much rain on the northern flank of the north African monsoon, strong wind biases over the sub-tropical north Atlantic and extratropical circulation biases to the southwest of southern Africa. The effect of the change in aerosol (Figure 2(c)) is a reduction in these particular biases so that they are no longer apparent in the systematic errors with the new aerosol (Figure 2(d)). Elsewhere, systematic errors are largely unchanged.

 doi:10.21957/345mr1psx6

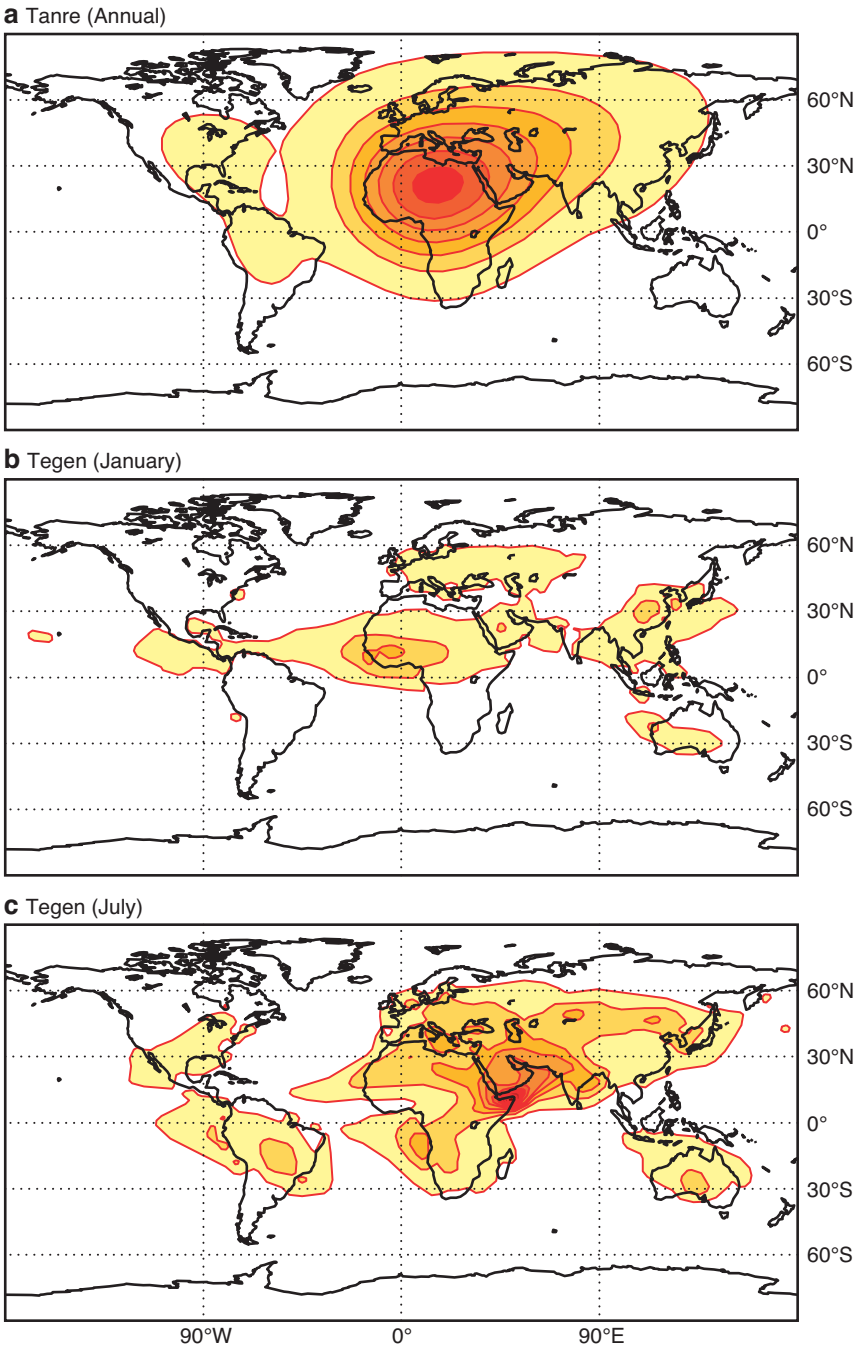

Figure 1 Optical depths at 550 nm associated with the model aerosol climatology. (a) The old annually-fixed climatology of *Tegen et al.* (1984). (b) The new January climatology of *Tegen et al.* (1997). (c) The new July climatology of *Tegen et al.* (1997).

doi:10.21957/345mr1psx6

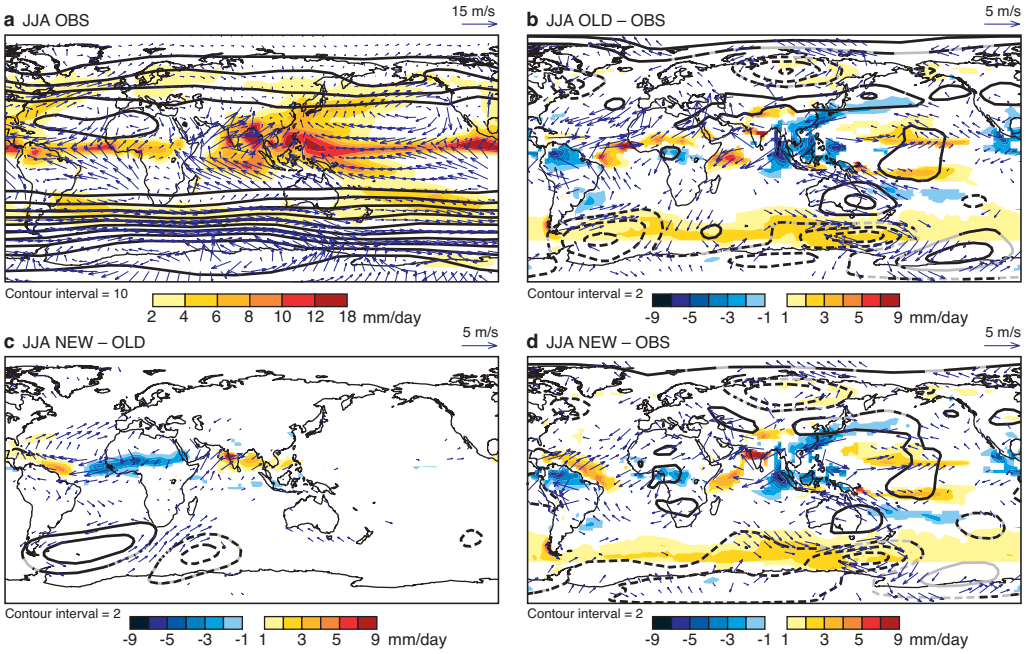

Figure 2 June–August total precipitation (shaded in mm day^{-1}), 925 hPa horizontal wind vectors (see scaling vector) and 500 hPa geopotential heights (contoured in dam). (a) From observations, with precipitation data coming from Xie-Arkin for the period 1980–1999 and the other fields from ERA-40 for the period 1962–2001. (b) Systematic error of model version Cy26r3 with old aerosol run at T95 resolution from 1 April for the years 1962–2001. (c) The difference between Cy26r3 with new aerosol and Cy26r3 with old aerosol. (d) Systematic error of model version Cy26r3 with new aerosol. Precipitation and wind differences are only plotted where they are statistically significant at the 10% level using a two-sided paired t-test taking autocorrelation into account. Height differences are contoured solid for positive, dashed for negative, grey where not significant and with contour interval indicated in each panel.

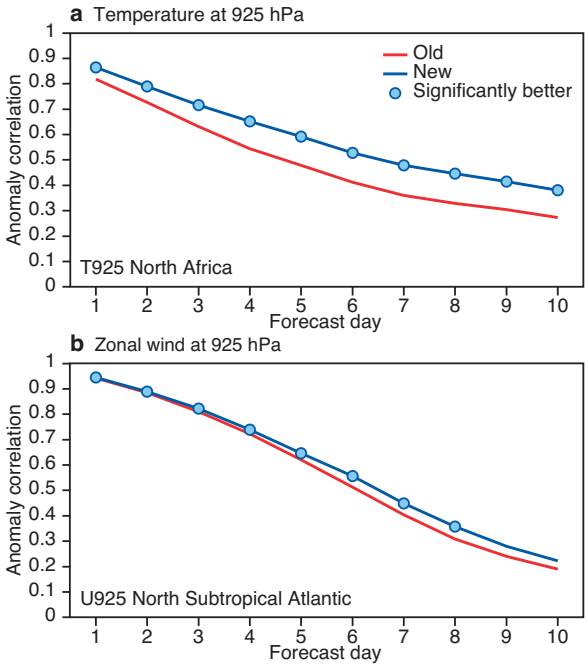

Figure 3 Mean anomaly correlations from T511 medium-range forecasts started each day in June–August 2003. (a) Temperature at 925 hPa over North Africa (20°W–40°E, 0°N–25°N). (b) Zonal wind at 925 hPa over the north subtropical Atlantic (80°W–10°W, 0°N–45°N). Red for the analysis/model version Cy26r1 (with old aerosol) and blue for Cy26r3 (with new aerosol). Dots indicate statistically significantly better forecast skill at the 10% level using a two-sided paired t-test taking autocorrelation into account.

doi:10.21957/345mr1psx6

Impact on medium-range forecast skill (June–August)

The model version Cy26r3 (with new aerosol) was tested at T511 resolution during June–August 2003 alongside the then operational version Cy26r1 (with old aerosol). Significant medium-range anomaly correlation skill improvements are apparent throughout the tropics in Cy26r3. Although there are several differences between these two analysis/model cycles, the major improvements in, for example, 925 hPa temperature over northern Africa (Figure 3(a)) (where a gain of 1.5 days is apparent for an anomaly correlation of 0.6) and in 925 hPa zonal wind over the subtropical north Atlantic (Figure 3(b)) (gain of 0.4 days) would appear to be predominantly due to the change in aerosol.

Understanding the local improvements

To better understand the physics that leads to these improvements it is useful to study the mean forecast "spin-up". If the model is not perfect, it is likely to have a somewhat different mean climate to that of the real world (or of the analyses). When averaged over many forecasts, the tendencies in the first few timesteps will reflect the adjustment from the climate of the analysis to the climate of the model. Moreover, since individual schemes within the model (convection, radiation, dynamics etc.) have not had time to fully interact with each other in the first few timesteps, it may be possible to break-down the complex physics involved in this adjustment and even identify the reasons for errors in the model climate.

To isolate the tendencies involved in the adjustment, one needs to remove the tendencies associated with the diurnal cycle. *Klinker and Sardeshmukh* (1992), who have previously used this "tendency budget" technique, removed the diurnal cycle by averaging the tendencies of forecasts started at four different times of the day (starting at 0, 6, 12 and 18 UTC). Tendency budget analysis was dropped when 4D-Var data assimilation was introduced because it was thought that the analysis would be too close to a valid model state to be able to detect any adjustment. This is partly the case (at least for the Amazon region that has been investigated in this respect) especially with a 12 hour (rather than 6 hour) data assimilation window. However by sampling the diurnal cycle more frequently it has been possible to estimate the adjustment more precisely and thus still use the methodology.

The mean tendencies are obtained from medium-range forecasts using model version Cy28r3 T255L60 with old and new aerosol. Forecasts were started every fifth day within June-August for 2003 and 2004 (a total of 38 forecasts) from operational analyses. These years were chosen because analyses in 2003 were made when the old aerosol was in operation and those in 2004 were made when then the new aerosol was in operation. Thus neither aerosol climatology should be favoured by the analysis. Diurnal averaging of "initial tendencies" is done between D+0.25 and D+1.25 and diurnal averaging of "balanced tendencies" is done between D+9 and D+10. Figure 4 shows vertical profiles of tendencies from the dominant schemes within the models, together with the total tendencies and the D+10 biases, averaged over the North African box 10°W–30°E, 5°N–30°N.

- Left column — initial temperature tendencies (D+0.25 to D+1.25).
- Middle column — balanced temperature tendencies (D+9 to D+10).
- Right column — initial humidity tendencies (D+0.25 to D+1.25).
- Top row — model with the old aerosol.
- Middle row — model with the new aerosol.
- Bottom row — difference between models with new and old aerosols (note the change in horizontal axis scaling).

All profiles include 70% confidence intervals (which take autocorrelation into account).

To a large extent, the initial temperature tendencies (Figure 4(a)) associated with the individual physical schemes balance each other. For example, in the mid-troposphere, convective heating (blue) tends to balance radiative cooling (dark green). This is an example of radiative-convective equilibrium. However, the total of the individual tendencies (red) is not quite zero and this reflects the climate adjustment. The tendency is for a warming of the lower troposphere (below about 500 hPa) and this is reflected in the D+10 bias (black) (although not below 884 hPa for which the bias must either develop before D+0.25 or after D+1.25: this is an important topic for future investigation and not affected by the aerosol change). The initial balance in lower-tropospheric humidity tendencies (Figure 4(c)) is between convective removal (blue) and dynamic supply (orange). Again the balance is not perfect and there is an initial moistening of the lower troposphere (red) which is clearly reflected in the D+10 bias (black). The destabilization of the upper-tropospheric thermal profile and stabilisation below (which is what one would expect intuitively from an excessive amount of aerosol) is likely to be the cause for the moistening of the lower troposphere and, in the balanced profiles (Figure 4(b)), the strong increase in upper-tropospheric convective heating (blue) and dynamical cooling (orange).

doi:10.21957/345mr1psx6

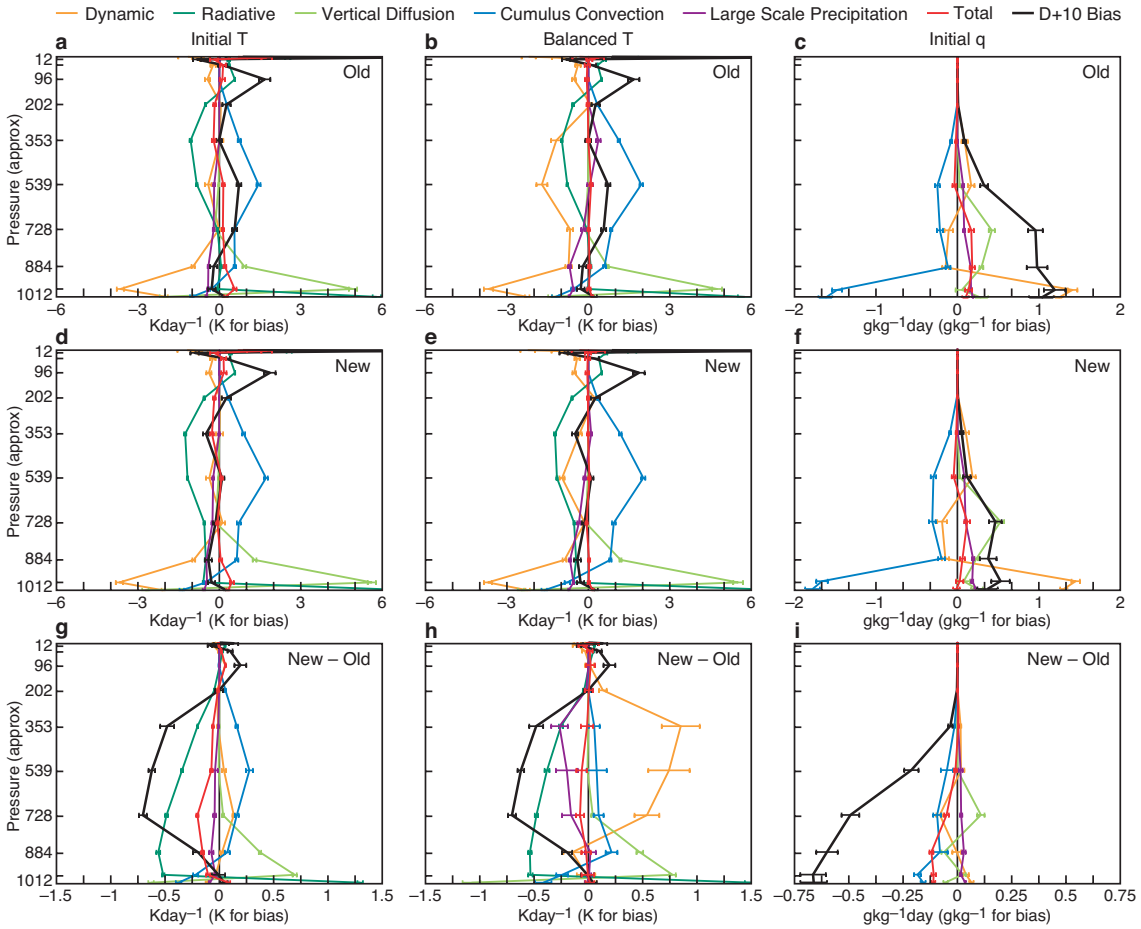

Figure 4 Vertical profiles of mean tendencies from the dominant physical schemes and the dynamics, together with total tendencies and D+10 biases (see key). 70% confidence intervals are indicated (taking autocorrelation into account). Model-level tendencies are obtained from 38 T255L60 forecasts started every fifth day during June-August for 2003 and 2004. The vertical axis shows approximate model level pressure and is linear in pressure. See captions or the main text for an explanation of the individual panels.

The total tendencies (and D+10 biases) from the model with the new aerosol (Figure 4, middle row) are generally much better than with the old aerosol (Figure 4, top row). In particular, the initial mid-tropospheric warming and D+10 warm bias have disappeared, the initial lower tropospheric moistening and D+10 moisture bias are halved and the balanced temperature tendencies are much more similar to the initial tendencies than was the case with the old aerosol.

The profile differences (Figure 4, bottom row) can help explain these improvements. The reduction in aerosol leads to less tropospheric shortwave absorption and more near surface heating (Figures 4(g) and 4(h), dark green). The initial differences for the other schemes are non-zero (Figure 4(g)). This indicates that over the first day these schemes have already begun to partially balance the radiative heating change. Nevertheless, the total tendency change (red) and D+10 bias change (black) do reflect the radiative forcing change. The destabilisation of the lower troposphere lowers the level from which initial convection can start and thus the convection is better able to remove the moisture supplied by the dynamics. Figure 4(i) shows this increased convective removal of moisture (blue) and the dramatic improvement in the D+10 biases (black).

An increase in convection throughout the troposphere (seen in the balanced temperature profile change, Figure 4(h), blue) may seem counter-intuitive since we have seen that the total precipitation actually decreases with the new aerosol (in these experiments D+10 area-mean precipitation reduces from 3.8 $mmday^{-1}$ to 2.9 $mmday^{-1}$, with an observed value from GPCP data of 2.7 $mmday^{-1}$). However, the increase in convection “feeds-off” the destabilised thermal profile and thus cannot entirely negate the radiative cooling effect of the aerosol change. Thus with the new aerosol there must be more descent (or less ascent), less large-scale moisture convergence and a reduction in large-scale precipitation. For moisture conservation, the reduction in large-scale precipitation must more than balance the increase in convective precipitation. All these features are evident in the balanced temperature profile changes (Figure 4(h)).

 doi:10.21957/345mr1psx6

D+10 zonal and meridional wind bias profiles (not shown) are also substantially (and statistically significantly) improved with the new aerosol. For example the 202 hPa meridional wind bias is reduced from –1.7 ms^{-1} to –0.2 ms^{-1} and the 884 hPa bias is reduced from +1.6 ms^{-1} to +0.8 ms^{-1}. These changes are consistent with the "local Hadley Circulation" change associated with the weakening and southward shift of the North African monsoon/ITCZ circulation. Further insight into the impact on the African Easterly Jet can be found in *Tompkins et al.,* 2004.

The tendency budget method provides a powerful and objective method of assessing changes to the model physics. Although a detailed analysis of the effects of the aerosol change has been given above, it should be noted that a simple assessment of the total initial tendencies is all that is required to determine whether a particular physics change is good or bad. Ideally, a separate data assimilation cycle should be made for each model version and each model initiated with its own analysis. This was not considered necessary here for the reasons stated above.

Impact on seasonal systematic errors (December–February)

Figure 5 shows climate simulation results for the December-February season based on forecasts started on 1 October for the years 1962–2001. The monsoons are now in the Southern Hemisphere (Figure 5(a)). The biases in the simulations with the old and new aerosols are shown in Figures 5(b) and 5(d), with the difference in the biases given in Figure 5(c). These results indicate that the aerosol change improves the precipitation biases over the tropical Atlantic and Indian Ocean, and (rather curiously due to its apparent disconnectedness) the height bias over the North Pacific. During this season the change in aerosol has a strong local impact on precipitation over the Gulf of Guinea. This is because, over the ocean, the atmospheric cooling associated with the reduced absorption of solar radiation is not balanced by surface sensible (or latent) heat fluxes as the ocean has a high heat capacity (it is infinite in these prescribed SST experiments). The dynamic adjustment to this cooling reduces the amount of moisture available to precipitate. The increase in precipitation to the east, over the Indian Ocean is consistent with an eastward upwelling Kelvin wave response to the Gulf of Guinea latent heating change although an additional local response to aerosol changes over the Indian Ocean itself has not been ruled-out at present.

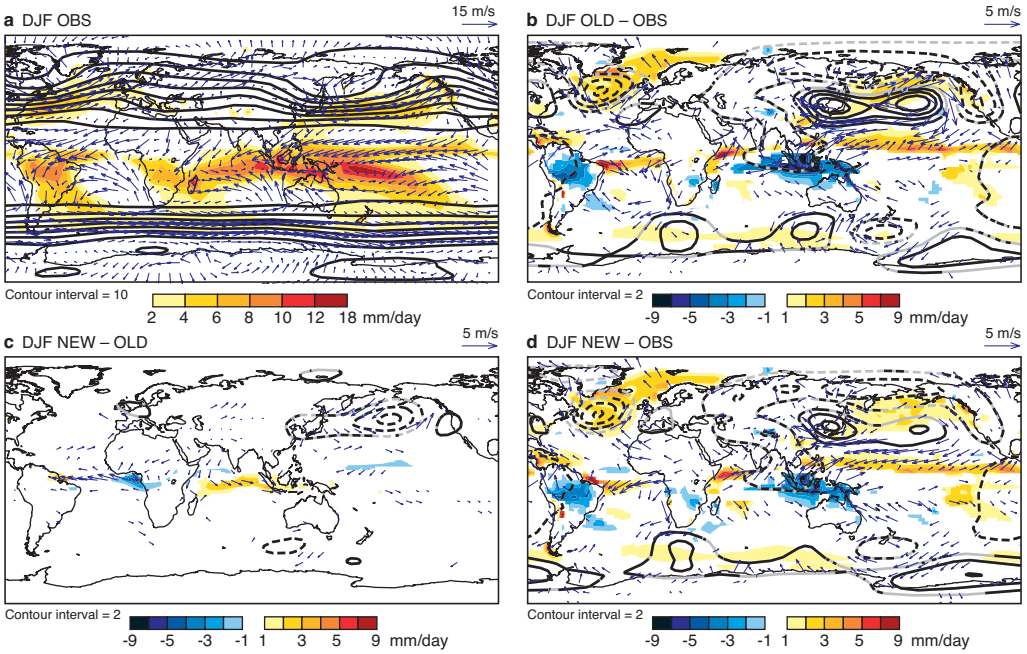

Figure 5 December–February total precipitation (shaded in mmday–1), 925 hPa horizontal wind vectors (see scaling vector) and 500 hPa geopotential heights (contoured in dam). (a) From observations, with precipitation data coming from Xie-Arkin for the period 1979/80–1998/99 and the other fields from ERA-40 for the period 1962–2001. (b) Systematic error of model version Cy26r3 with old aerosol run at T95 resolution from 1 October for the years 1962–2001. (c) The difference between Cy26r3 with new aerosol and Cy26r3 with old aerosol. (d) Systematic error of model version Cy26r3 with new aerosol. Precipitation and wind differences are only plotted where they are statistically significant at the 10% level using a two-sided paired t-test taking autocorrelation into account. Height differences are contoured solid for positive, dashed for negative, grey where not significant and with contour interval indicated in each panel.

doi:10.21957/345mr1psx6

Understanding the global improvements

To better understand the North Pacific pressure bias improvement, Figure 6 shows 250 hPa seasonal simulation differences (new minus old aerosol) in stream function (thick contoured), divergent wind (vectors) and "Rossby Wave Source" (shaded), *Sardeshmukh and Hoskins* (1988). The anomalous upper-level convergence over the Gulf of Guinea, associated with the precipitation decrease, and divergence over the Indian Ocean (and associated convergence to the north) are clearly evident. In addition, the strong reduction in aerosol over the Sahara (compare Figures 1(a) and 1(b)) leads to a radiative cooling anomaly (not shown). Although there is no precipitation for this forcing to positively feed-back with at this time of year, the radiative cooling alone is apparently enough to force considerable descent and upper-level convergence. The upper-level divergence field associated with all these features and the advection of mean absolute vorticity (mean absolute vorticity is shown with thin grey contours) by the divergent wind leads to Rossby wave forcing (shading) along the Northern Hemisphere subtropical jet. The apparently disconnected North Pacific pressure bias improvement is now seen (rather beautifully!) to be part of the barotropic Rossby wave response to this vorticity forcing.

Note that for June–August, the tropical upper tropospheric stream function and Rossby Wave Source biases are greatly improved with the new aerosol; with the remaining source of error centred around the Philippine Sea region (not shown). The extratropical responses for both June-August (Figure 2) and December-February (Figure 5) are predominantly limited to the winter hemisphere. It is possible that the upper-level out-flow associated with tropical convective anomalies is stronger in the winter hemisphere (as is the case for the mean Hadley Circulation) and has a stronger impact on vorticity forcing owing to the stronger winter vorticity gradients.

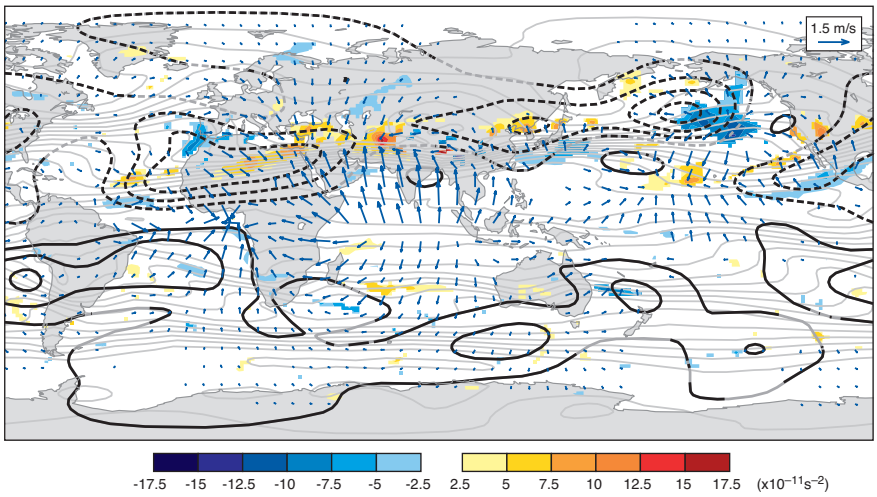

Figure 6 The difference between Cy26r3 with new aerosol and Cy26r3 with old aerosol in terms of the 250 hPa divergent wind vectors, stream function (contoured thick – contour interval $2x10^{6}$ $m^{2}s^{-1}$) and Rossby Wave Source (shaded – contour interval of $2.5x10^{-11}$ s^{-2}). Also shown is the mean (i.e. (old+new)/2) absolute vorticity (contoured thin grey with interval $1x10^{-5}$ s^{-1}). Differences in divergent wind and Rossby Wave Source are only plotted where significant at the 10% level. Streamfunction differences are contoured solid where positive, dashed where negative and grey where not significant.

doi:10.21957/345mr1psx6

Future use of observed and interactive aerosol

We have seen that changes in aerosol can have a strong impact on local precipitation and the global circulation. This effect is apparent not only in seasonal forecasts but also in the medium- range. This being so, what would be the impact of using observed aerosol? Seasonal forecast sensitivity experiments have been carried out in which the new (Tegen) aerosol was replaced with MODIS satellite-derived aerosol optical depths. Over Asia this did not lead to such large changes in the local or global circulation in June-August. This may reflect the smaller and more local change in aerosol or highlight the importance of a strong interaction with precipitation in order to magnify the aerosol effect. Nevertheless, the results above indicate that it is possible that the future use of observed aerosol and the incorporation of an interactive aerosol scheme could lead to further forecast skill improvements.

Further reading

Klinker, E. & **P.D. Sardeshmukh, 1992:** The diagnosis of mechanical dissipation in the atmosphere from large-scale balance requirements. *J. Atmos. Sci.,* **49,** 608–627.

Sardeshmukh, P.D. & **B.J. Hoskins, 1988:** The generation of global rotational flow by steady idealized tropical divergence. *J. Atmos. Sci.,* **45,** 1228–1251.

Tanre, D., J-F. Geleyn & **J.M Slingo, 1984:** First results of the introduction of an advanced aerosol-radiation interaction in the ECMWF low resolution global model. In *Aerosols and Their Climatic Effects.* H.E. Gerber and A. Deepak, Eds., A. Deepak Publ., Hampton, Va., 133–177.

Tegen, I., P., Hollrig, M. Chin, I. Fung, D. Jacob & **J. Penner, 1997:** Contribution of different aerosol species to the global aerosol extinction optical thickness: Estimates from model results. *J. Geophys. Res.,* **102,** 23895–23915.

Tompkins, A.M., C. Cardinali, J-J. Morcrette & **M.J. Rodwell, 2004:** Influence of aerosol climatology on forecasts of the African Easterly Jet. *Geophys. Res. Lett.,* **32,** doi:10.1029/2004GL022189.

doi:10.21957/345mr1psx6